


Performance of biocomposites from surface modified regenerated cellulose fibers and lactic acid thermoset bioresin

Sunil Kumar Ramamoorthy · Fatimat Bakare ·
Rene Herrmann · Mikael Skrifvars 

Received: 4 February 2015 / Accepted: 29 April 2015
© Springer Science+Business Media Dordrecht 2015

Abstract The effect of surface treatments, silane and alkali, on regenerated cellulose fibers was studied by using the treated fibers as reinforcement in lactic acid thermoset bioresin. The surface treatments were performed to improve the physico-chemical interactions at the fiber-matrix interface. Tensile, flexural and impact tests were used as indicator of the improvement of the interfacial strength. Furthermore, thermal conductivity, viscoelasticity measurements as well as microscopy images were made to characterize the fiber surface treatments and the effect on adhesion to the matrix. The results showed that silane treatment improved the mechanical properties of the composites as the silane molecule acts as link between the cellulose fiber and the resin (the fiber bonds with siloxane bridge while the resin bonds with organofunctional group of the bi-functional silane molecule) which gives molecular continuity in the interphase of the composite. Porosity volume decreased significantly on silane treatment due to improved interface and interlocking between fiber and matrix. Decrease in water absorption and increase in contact angle con-

firmed the change in the hydrophilicity of the composites. The storage modulus increased when the reinforcements were treated with silane whereas the damping intensity decreased for the same composites indicating a better adhesion between fiber and matrix on silane treatment. Thermogravimetric analysis indicated that the thermal stability of the reinforcement altered after treatments. The resin curing was followed using differential scanning calorimetry and the necessity for post-curing was recommended. Finite element analysis was used to predict the thermal behavior of the composites and a non-destructive resonance analysis was performed to ratify the modulus obtained from tensile testing. The changes were also seen on composites reinforced with alkali treated fiber. Microscopy images confirmed the good adhesion between the silane treated fibers and the resin at the interface.

Keywords Surface modification · Cellulose fiber · Mechanical properties · Thermal conductivity · Finite element analysis · Resonance analysis

S. K. Ramamoorthy · F. Bakare · M. Skrifvars (✉)
Swedish Centre for Resource Recovery, University of
Borås, 501 90 Borås, Sweden
e-mail: Mikael.Skrifvars@hb.se

R. Herrmann
Department of Energy and Materials Technology, Arcada
University of Applied Science, 00560 Helsinki, Finland

Introduction

Natural fiber reinforced composites have shown significant importance in the composite industry and the good reinforcing potential of these fibers has led to extensive use of these composites in automotive applications (Jawaid and Abdul Khalil 2011; La

Mantia and Morreale 2011; Faruk et al. 2012; Bledzki and Gassan 1999; Koronis et al. 2013; Puglia et al. 2005). The use of cellulosic fibers obtained from bast, leaf, seed, wood, straw and grass as reinforcements in plastics has increased in recent decades (Faruk et al. 2012; Ramamoorthy et al. 2015). Natural fibers have good physical and mechanical properties, which make them a right choice as low cost reinforcement (Faruk et al. 2012; Bledzki and Gassan 1999; Ramamoorthy et al. 2015). However, the hydrophilicity due to the cellulosic hydroxyl groups and surface unevenness make natural fibers less preferred over synthetic fibers such as glass fibers in more demanding composite applications. The mechanical processing from field to fiber includes several stages (growing, field retting, scotching, hackling, carding and spinning), this makes the processing both costly, and also prone to quality fluctuations (Jawaid and Abdul Khalil 2011; Faruk et al. 2012). Regenerated or partly man-made cellulose fibers do not have these drawbacks.

Researchers have used regenerated cellulosic fibers as an alternate to the natural fibers in fiber reinforced composites (FRC); as the primary constituents' of both the fibers remains the same. Regenerated cellulose fibers are chemically pure, their surface structure is even, and the fiber properties can be reproduced easily (Woodings 2001; Carrillo et al. 2010; Adusumali et al. 2006; Fink et al. 2014). It is also found that these fibers have good potential to be used as reinforcement in FRC (Carrillo et al. 2010; Adusumali et al. 2006; Ganster and Fink 2006; Jaturapiree et al. 2006). High surface evenness and even quality of these fibers makes it possible to get consistent results which are not possible in natural fiber (Woodings 2001). These fibers are unique, as they possess the beneficial properties of both natural and synthetic fibers (Johnson et al. 2008). They have low density, which give low weight composites, their environmental characteristics are like as for natural fibers, and their performance is stable like as for synthetic fibers (Johnson et al. 2008).

Our previous studies show the great potential of regenerated cellulose fibers as reinforcements in FRC, and these could be a good alternative for annual plant fibers (Ramamoorthy et al. 2012, 2013, 2014). The mechanical properties of composites reinforced with regenerated cellulose are better than for several natural fiber composites (Carrillo et al. 2010; Ramamoorthy et al. 2012, 2013; Saevey et al. 2001).

In recent years, the synthesis of biothermosets has been reported. The matrix is synthesized from renewable constituents such as soybean or linseed oil, or from lactic acid (Seniha Güner et al. 2006; Åkesson et al. 2010). The properties of synthesized matrixes from renewable resources have been explored by researchers and proven to be good alternative to petroleum based matrixes in natural fiber reinforced composites (Åkesson et al. 2011; Adegunle et al. 2011). Reinforcements and matrix resins made from renewable resources have been claimed to have environmental and economic benefits such as low pollutant emissions, low greenhouse gas emissions and low cost (La Mantia and Morreale 2011). Researchers are therefore aiming to produce green composites for several applications from renewable reinforcement and matrix (La Mantia and Morreale 2011).

However, there are several issues involved when using polar hydrophilic fibers with non-polar hydrophobic matrixes in the production of biocomposites, and the most important issue is the interface between fiber and matrix (John and Anandjiwala 2008). Cellulosic fibers have polar OH groups in each glucan unit and can readily absorb moisture or water while the thermoset matrixes derived from lactic acid are nearly hydrophobic which causes poor fiber–matrix interface due to poor fiber wetting (Caulfield et al. 1999). The mechanical properties of the composites are directly affected by the interfacial adhesion as the load transfer takes place by shear stresses at the interface (Caulfield et al. 1999). Poor fiber–matrix adhesion in the interface results in improper transfer of load and thus reducing the full capabilities of the composite (Caulfield et al. 1999). Therefore, the natural fibers are often modified, physically or chemically, to attain good interface, which improves mechanical performance of the composites (Mohanty et al. 2001; Bledzki et al. 1996).

Chemical treatments such as silane and alkali are common and straight forward methods to modify the surface of the natural fibers which has improved the properties (Mohanty et al. 2001). Such treatments also roughen the surface of the fiber, which improves the mechanical bonding and thus stress transfer at interface is appreciable (Mohanty et al. 2001). Alkali treatment disrupts the intermolecular hydrogen bonding in the cellulose fiber bundle and removes certain

parts (lignin, hemicellulose, wax and oil) of the fibers, which alter the fiber surface (Mohanty et al. 2001). Silane treatment acts as a coupling agent that may reduce the number of hydroxyl groups in the fiber–matrix interface by reaction with the silica molecules (Ramamoorthy et al. 2014). These changes in the fibers' surface could improve the mechanical properties of the fibers due to change in structural changes (John and Anandjiwala 2008). The fiber–matrix interface is also affected by the change in the fibers' characteristics as the physico–chemical interactions between fiber and matrix will be altered (Mohanty et al. 2001).

Our previous studies show that the mentioned treatments improve the surface roughness and the performance of the fibers for composite applications (Ramamoorthy et al. 2014); and will result in a good reinforcement for of the lactic acid based biomatrix (Bakare et al. 2014). A untreated regenerated cellulose reinforced soybean-based thermoset composites show even a better performance than some natural fiber composites (Faruk et al. 2012; Carrillo et al. 2010; Ramamoorthy et al. 2012, 2013). This is mainly attributed to superior fiber properties. Microscopic images indicated that these composites were porous; and the unevenness in matrix impregnation resulted in delamination (Ramamoorthy et al. 2013). The absence of chemical treatment leads to poor interface between fiber and matrix (Caulfield et al. 1999; Mohanty et al. 2001; Bledzki et al. 1996). In recent study regenerated cellulose fibers were treated by silane and alkali and the treatment conditions such as treatment time, treatment temperature and concentration of the treatment solution were studied. Testing of the treated fibers revealed better properties of some of the treated fibers than untreated fibers. Harsh treatment conditions lead to fibrillation of fibers, which resulted in poor mechanical performance (Ramamoorthy et al. 2014). Biomatrix from lactic acid has been synthesized and characterized in our prior study which revealed the good potential of the matrix in composite industry (Bakare et al. 2014).

In this paper, composites are produced from surface treated regenerated cellulose fibers and a lactic acid thermoset resin. The composite performance is evaluated through mechanical, thermal, viscoelastic and morphological properties.

Experimental

Materials

Viscose nonwoven fabrics with 60 g/m² surface weight and made from 1.7 dtex linear density regenerated cellulose staple fibers were supplied by Suominen Nonwovens Ltd, Finland. Reagent grade sodium hydroxide pellets, L-lactic acid (88–92 %) and glycerol (99.5 %) were obtained from Scharlau, Spain. APTES, 3-aminopropyl-triethoxysilane (99 %), toluene (99.9 %), absolute ethanol (≥ 99.8 %), ethylene glycol (99.8 %), formamide (≥ 99.5 %) and hexadecane (>99 %) were supplied by Sigma Aldrich, USA. Dibenzoyl peroxide initiator (>98 %) and hydroquinone (99 %) were supplied by Kebo Lab, Sweden and Acros Organics respectively. Methanesulfonic acid (≥ 98 %) and methacrylic anhydride were supplied by Alfa Aesar.

Treatment

Alkali treatment

Regenerated cellulose fabrics were pre-dried at 105 °C before immersing in three different concentrations (6, 8 and 10 wt%) of sodium hydroxide (NaOH) solutions for 30 min at room temperature. After the treatment, fibers were washed thoroughly with distilled water until neutrality. The pH was checked periodically using litmus paper. Then the fibers were dried in room temperature followed by oven drying for 3 h at 105 °C. Fiber behavior on alkali treatment was studied in previous research (Ramamoorthy et al. 2014; Jaturapiree et al. 2006; Okubayashi and Bechtold 2005).

Silane treatment

Pre-dried regenerated cellulose fabrics were immersed in three different silane concentration solutions (6, 8 and 10 wt%) at room temperature for 30 min. APTES (3-aminopropyl-triethoxysilane) was used as silane coupling agent and was added to ethanol–water mixture (8:2 volume ratio) to treat the regenerated cellulose fabrics. Fibers were washed thoroughly with distilled water after treatment and pH was checked for neutrality. Then the fibers were dried in room

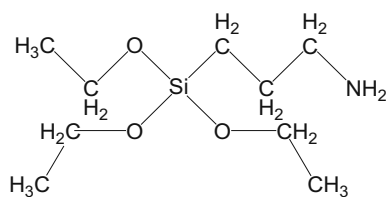


Fig. 1 Structural formula of 3-aminopropyl-triethoxysilane ($C_9H_{23}NO_3Si$)

temperature followed by oven drying for 3 h at 105 °C (Fig. 1).

In our previous research, the spectral changes were followed by Fourier transform infrared spectroscopy (FTIR) and Raman spectroscopy, which confirmed the changes in the surface chemistry of the fibers on silane and alkali treatments (Ramamoorthy et al. 2014). Detailed investigation on treated fibers was presented in our preceding study (Ramamoorthy et al. 2014).

Resin synthesis

The synthesis was done according to the procedure discussed thoroughly in our earlier work (Bakare et al. 2014). Lactic acid and glycerol were reacted in a direct condensation; the product was then end-functionalized with methacrylic anhydride. The reaction was done in a 3-neck flask, equipped with a Dean-Stark distilling head and a condenser. In the first step, 0.12 mol of glycerol was added to 1.08 mol of lactic acid diluted in

50 g of toluene. Methanesulphonic acid, 0.1 wt%, was used as catalyst. The condensation reaction took place for totally about 5 h, first 2 h at 145 °C, followed by 2 h at 165 °C and 1 h at 195 °C. In the second step, the product was cooled to 110 °C and end-functionalized with 0.396 mol of methacrylic anhydride. The end-functionalization proceeded for about 4 h. Both reaction steps were done under nitrogen atmosphere. The resin was obtained by removing the residual methacrylic acid that had formed after the second step together with toluene using rotary evaporator distillation at a temperature of 60 °C and a pressure of 13 mbar.

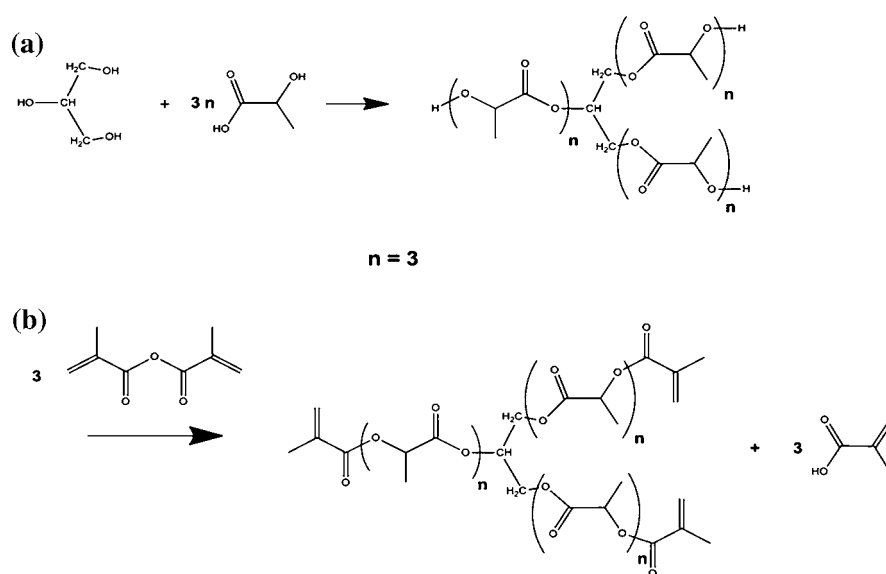
Figure 2 shows the two reactions, condensation and functionalization, during resin synthesis. The viscosity of the resin was 1.09 Pa s. The bio content was calculated according to ASTM D6866 using the equations:

$$\text{Bio content} = \frac{\text{bio carbon content}}{\text{total carbon content}} \times 100 \quad (1)$$

$$\text{Bio content} = \frac{[G_m + 3n(L_m - W_m)]}{G_m + 3[(MA_m - M_m) + n(L_m - W_m)]} \times 100 \quad (2)$$

where G_m is the weight of glycerol, n is the chain length, L_m is the weight of lactic acid, W_m is the weight of the water condensed, MA_m is the weight of methacrylic anhydride and M_m is the weight of the

Fig. 2 Resin synthesis reaction. **a** Condensation reaction, **b** methacrylic functionalization



methacrylic acid formed (Bakare et al. 2014). Based on this equation, it was found that the resin had 78 % bio content.

The ^{13}C -NMR results presented in our previous paper showed that 90.2 % lactic acid reacted with glycerol whereas 8.9 % reacted into lactic acid oligomers and 0.9 % formed a lactide. The chain length of the polymer and the lactic acid oligomers were 4 and the 2.2 respectively. Functionalization with methacrylic anhydride in the second step was verified using Fourier transform infrared (FTIR).

Composite preparation

The regenerated cellulose fabrics, untreated and treated, were cut to $20 \times 20 \text{ cm}^2$ dimension. Resin viscosity has a major role in fiber impregnation and the viscosity was therefore reduced by heating the resin in an oven at $60 \text{ }^\circ\text{C}$ for 5 min. Dibenzoyl peroxide (2 wt%) was used as initiator and was mixed well with the heated resin to get a homogeneous mixing. The fiber–matrix weight ratio of about 1:1 was chosen due to good resin impregnation. The impregnated fabrics were then stacked between two steel plates and pressed in a manual hot press. The curing was done at a temperature of $150 \text{ }^\circ\text{C}$ and at a pressure of 40 bar. The hot press used for the compression molding was supplied by Rondol Technology, Staffordshire, UK.

Specimen preparation

Specimens were cut from the composite laminates using laser-cutting technology, GCC LaserPro Spirit (Taiwan), for below mentioned tests according to ISO standards. The specimens were cut from the centers of the composite laminates, leaving the edges to minimize edge effects.

Characterisation

Tensile test

Tensile tests were carried out according to ISO 527 using a Tinius Olsen H10KT universal testing machine and QMat software. The dumb bell shaped tensile test specimens were clamped and pulled apart; using a 10 kN load cell and a mechanical extensometer. The overall length of the specimen was 150 mm which

includes 60 mm parallel sided portion. The parallel sided portions' width was 10 mm and the width at the ends was 20 mm. The gauge length was 50 mm and the rate of loading was 10 mm/min. The tensile properties such as tensile strength, E-modulus and % elongation were studied. Ten specimens were tested for each batch and the average is noted.

Impact test

The Charpy impact test was performed according to ISO 179 using a digital Zwick test instrument. The flat and un-notched specimens were tested flatwise. Ten specimens were tested for each batch and the average impact resistance is noted.

Flexural test

The three point flexural tests were carried out according to ISO 14125 using Tinius Olsen H10KT universal testing machine and QMat software. The flat specimens, $80 \times 15 \text{ mm}^2$ (length \times width), were placed with support at two ends and the force was applied in the middle; and this force was detected by load cell (10 kN). The outer span was 64 mm and the rate of loading was 10 mm/min. The flexural properties such as flexural strength and modulus were investigated. Five specimens were tested for each batch and the average is noted.

Density and porosity measurements

Archimedes principle, buoyancy method, was used to determine the densities of the composite specimens. The specimens were covered with paraffin before immersing in ethanol medium to avoid absorption. The porosity was calculated using the method suggested by Madsen et al. (2007). At least three measurements were done for each sample and the average is reported.

Dynamic mechanical thermal analysis (DMTA)

Dynamic mechanical thermal analysis was carried out using Q series DMTA, TA Instrument, supplied by Waters LLC, USA. The specimen dimension was $30 \times 10 \text{ mm}^2$ (length \times width), and it is mounted in dual cantilever clamp. The temperature range was between 20 and $150 \text{ }^\circ\text{C}$ at a frequency of 1 Hz. The

storage modulus, loss modulus and $\tan \delta$ were studied to evaluate the viscoelastic performance of the composites. The measurements were done at least twice for each sample.

Differential scanning calorimetry (DSC)

Differential scanning calorimetry analysis was carried out using Q series DSC, TA Instrument, supplied by Waters LLC, USA. Approximately 10 mg of composite sample sealed in aluminum pan was heated from 20 to 200 °C at a rate of 10 °C/min. The sample is cooled to 20 °C and heated again to 200 °C. The analysis was done under nitrogen. The measurements were done at least twice for each sample. DSC was also used to measure specific heat capacity (C_p) of the fiber and the cured resin. The instrument was calibrated with standard sapphire material before the experimentation, at the temperature range of 0 and 54 °C, at a heating rate of 10 °C/min. Measurements were done twice with approximately 13 mg sample in nitrogen atmosphere.

Thermogravimetric analysis (TGA)

Thermogravimetric analysis was carried out using Q series TGA, TA Instrument, supplied by Waters LLC, USA. The sample weighing approximately 15 mg was heated from 30 to 600 °C in platinum pan at a heating rate of 10 °C/min under nitrogen atmosphere. The measurements were done at least twice for each sample and the average is reported.

Contact angle and surface energy

The contact angle measurement was done on optical tensiometer from Attension, Theta Lite (Espoo, Finland) equipped with appropriate software. A liquid drop is placed on flat surface of the composite and the contact angle is measured using camera by assessing shape of the drop. The contact angle is directly measured from the angle formed between the composite sample and the tangent to the drop surface. Four wetting agents such as water (WA), ethylene glycol (EG), formamide (FO) and hexadecane (HD) were used. The contact angles and the surface energies of the composites reinforced with untreated and treated

fibers were measured. At least seven measurements were done for each sample and the average is reported.

Water absorption

Gravimetric water absorption tests were carried out on the composites ($36 \times 12 \text{ mm}^2$), by immersing in water for 10 days to determine the hydrolytic stability of the composites. The specimens were dried and weighed before placing in the distilled water at room temperature and pressure. The amount of water absorbed was measured everyday by taking out the specimen and carefully drying the specimen surface before weighing. The thickness of the specimens was measured on a daily basis to study the stability. The percentage water absorption (WA%) and thickness increase were studied. At least three measurements were done for each sample and the average is reported.

Microscopy

Morphological analysis was performed on cross-section of tensile fractured specimens using optical and scanning electron microscope (SEM). The optical microscope was supplied by Nikon Instruments (Japan) and the images were taken directly on cross-section without any preparation. Scanning electron microscope images were taken on AIS2100 (Seron Technology, Korea) at 20 kV accelerated voltage after the specimens were sputtered with a layer of gold.

Resonance analysis

Resonance frequency after bending the specimen was obtained by a non-destructive method using a composite cantilever beam. The apparatus for the analysis was self-constructed by attaching a piezo electric transducer to the beam which was connected to a laptop's sound card via 2.5 mm audio jack after passing through high pass filter in series. The beam was excited by bending, and the acoustic signals were received using Audacity software. The signals were converted to frequency and further analyzed using Scilab 5.5.0 numerical computational software. This is compared to the Young's modulus obtained by the mechanical testing.

The Young's modulus is calculated using the following equation,

$$\omega = \sqrt{\frac{k}{m}} = \alpha^2 \sqrt{\frac{EI}{\lambda L^4}} \quad (3)$$

where E is the young's modulus, I is the moment of inertia of a beam, λ is the linear mass density and L is the length of the beam. This can be re-arranged to find the Young's modulus,

$$E = \left(\frac{\lambda}{I}\right) \left(\frac{A}{\alpha^2}\right)^2 \quad \text{where } A = \alpha^2 \sqrt{\frac{EI}{\lambda}} \quad (4)$$

Using this equation, $E = \left(\frac{\lambda}{I}\right) \left(\frac{A}{\alpha^2}\right)^2$, the modulus was calculated; λ was calculated by measuring the mass and length of the beam, the I of the beam was calculated using thickness and width $\left(\frac{\text{width} \times \text{thickness}^3}{12}\right)$, A was the slope obtained from the Fig. 7c and α is constant value, 1.875.

Code executed in Scilab 5.5.0 from audio signals obtained from Audacity,

```

"D=fscanfMat('naoh8.csv');
dt=1/8000;
t_max=max(size(D));
T=0:1:T_max-1;
t=t*dt;
//compute the fft
y=fft(D,-1);
spectrum=ffshift(abs(y));
//display
xset("window",0)
xgrid(0)
plot2d(t,D,2)
xset("window",1)
xgrid(0)
frequency=0:1/max(t):(max(size(t))-1)/max(t);
plot2d(frequency-0.5*max(frequency),
2*spectrum/max(size(t)),2,rect=[0,0,max(frequency)/2,2*max(spectrum)/max(size(t))])"

```

Thermo-physical test

Thermo-physical study was performed according to ISO 22007 on transient plane source (TPS) 2500 hot disk (Hot Disk AB, Gothenburg, Sweden) equipped with suitable software at room temperature and pressure. The specimen dimension was $50 \times 10 \text{ mm}^2$ and thickness was between 3 and 4 mm. The heating power and the measurement time were 50 mW and 10 s. Two identical specimens were used

for each measurement; one above the sensor and another underneath the sensor. The heat source is used to heat the specimen and the data is collected from both the specimens at the same time. The software reported the average thermal properties of the two specimens. Thermal conductivity, thermal diffusivity and volumetric specific heat were measured simultaneously. At least three measurements were done for each sample and the average is reported.

Thermal conductivity can also be calculated using Bruggman's model,

$$\frac{(\lambda_e - \lambda_f)(\lambda_m)^{\frac{1}{3}}}{(\lambda_m - \lambda_f)(\lambda_e)^{\frac{1}{3}}} = (1 - v) \quad (5)$$

where λ_f and λ_m are thermal conductivity of the fiber and matrix respectively, λ_e is the efficient thermal conductivity of the composite.

Finite element analysis

Finite element analysis software, COMSOL 4.3b, was used to predict the temperature rise generated in the composites during the heating experiments. The specific heat capacity of the fiber and cured resin was obtained from the DSC analysis and was used to simulate the experimental method. The temperature distribution for the composite during heating was calculated by a Fourier heat conduction equation:

$$\rho C_p \frac{\partial T}{\partial t} = k_x \frac{\partial^2 T}{\partial x^2} + k_y \frac{\partial^2 T}{\partial y^2} + k_z \frac{\partial^2 T}{\partial z^2} \quad (6)$$

where ρ is the density and C_p is the specific heat capacity of the composite; and k_x , k_y and k_z are thermal conductivity coefficients in main axes. For the nonwoven (unidirectional) composites, the thermal conductivity in machine direction can be calculated by the rule of mixtures

$$k_c = v_f k_f + (1 - v_f) k_m \quad (7)$$

where k_c , k_f and k_m are thermal conductivity of the composite, fiber and matrix; and V_f is fiber volume fraction.

Results and discussion

The change in chemical composition and the crystallinity after silane and alkali treatments on cellulose fibers were reported in a former study using FTIR and Raman spectroscopy (Ramamoorthy et al. 2014). Mechanical (tensile strength, modulus and elongation) and thermal (heat capacity and stability) properties of the treated fibers were investigated. Further, weight loss, swelling and moisture absorption were examined.

The hydrophilicity of these fibers was assessed by contact angle measurements and 114° was attained on silane treatment. SEM images showed the increase in surface roughness and fibrillation on different fiber treatments (Ramamoorthy et al. 2014). The treated cellulose fibers were used to reinforce a synthesized thermoset resin, and the obtained composites were characterized in this study.

Tensile, flexural and impact properties were determined to see the mechanical performance of the composites, in order find out the potential applications.

Tensile test

Table 1 shows tensile strength, Young's modulus and elongation for the different composite types. Nonwoven composites were tested in machine direction and the tensile strength of the composites was between 60 and 100 MPa which falls in line with previously reported nonwoven fiber reinforced lactic acid based thermoset composites (Esmaili et al. 2014). Our former study showed that soybean oil based thermoset nonwoven fiber composites had tensile strength between 70 and 100 MPa at 40–60 wt% fiber loading (Ramamoorthy et al. 2012, 2013). Tensile modulus of the composites was between 6 and 10 GPa while the

Table 1 Tensile and impact properties of the composites with various treated conditions

Sample conditions	Tensile strength (MPa)	Young's modulus (GPa)	Elongation (%)	Impact strength (kJ/m ²)
Untreated ^a	80.86 ± 6.28	7.80 ± 1.41	2.22 ± 0.18	18.56 ± 1.60
Silane treated				
6 wt%	82.41 ± 3.82	8.24 ± 0.83	1.68 ± 0.20	19.36 ± 2.51
8 wt%	85.67 ± 4.33	8.30 ± 2.04	1.59 ± 0.16	26.01 ± 3.51
10 wt%	91.43 ± 4.69	9.52 ± 1.89	1.24 ± 0.31	27.98 ± 2.46
Alkali treated				
6 wt%	83.64 ± 5.57	8.10 ± 1.61	0.91 ± 0.20	23.78 ± 2.33
8 wt%	71.76 ± 5.93	7.83 ± 1.84	0.75 ± 0.18	18.93 ± 2.42
10 wt%	60.32 ± 7.82	6.90 ± 2.09	0.46 ± 0.10	16.92 ± 2.57
Thermally treated ^b at 140 °C for 2 h (post-curing)				
Untreated	79.15 ± 3.67	7.71 ± 1.35	2.11 ± 0.16	18.81 ± 1.34
Silane 10 wt%	96.29 ± 3.28	9.70 ± 1.64	1.16 ± 0.23	29.52 ± 3.80
Alkali 6 wt%	86.62 ± 5.10	8.56 ± 1.93	0.85 ± 0.19	24.47 ± 2.48

Standard deviation written after ±

^a No post curing

^b Thermal treatment

maximum elongation was about 2.1 %, which follow the results from our earlier studies (Ramamoorthy et al. 2012, 2013; Esmaeili et al. 2014). Further, acoustic emissions could be used to analyze microstructural damage analysis (Bravo et al. 2015).

Tensile strength and modulus increased when the fibers were treated with silane. Similar improvements on silane treatments have been reported before (Faruk et al. 2012; John and Anandjiwala 2008; Mohanty et al. 2001). The changes were primarily due to the amino functional silane, which not only alter the hydrophilicity of the cellulose fibers but also react with the resin in the interface. According to the chemical bonding theory, the bifunctional silane molecules act as a link between the cellulose fiber and the resin; by forming a bond with fiber surface through a siloxane bridge while its organofunctional group bonds to the resin which gives molecular continuity across the interface region of the composite. Even at high silane concentration (10 wt%), the tensile strength and the modulus of the composites in this study did not reach 100 MPa and 10 GPa respectively. This could be due to saturation of the interacting bonds (fiber–Si–resin) and the textile architecture of the reinforcement. As expected, the tensile elongation of the composites decreased when the fibers were treated with silane as the interface between fiber and matrix was improved.

Tensile properties of alkali treated fiber reinforced composites were dependent on concentration of the alkali treatment; low concentration slightly increased the strength and modulus of the composites whereas high concentration decreased the tensile properties. This marginal increase cannot be discussed due to high standard deviation but the decrease was evident with 33 % lower tensile strength for highest alkali concentration (10 wt%). This follows our preceding research on alkali treatment on fibers where severe fibrillation of fibers occurred at high concentration treatment (Ramamoorthy et al. 2014). At low concentration, the alkali treatment disrupts the hydrogen bonding in the cellulose network and increases the surface roughness, and good adhesion characteristics were expected when reinforced in the matrix. The elongation of the composites decreased with increasing alkali concentration due to increased fiber splitting/fibrillation. A small increase of surface roughness, pore formation and fibrillation in fibers due to the alkali treatment could improve the composite properties as the pores

on the fiber surface allow for good interlocking with the matrix, whereas, high degree of pore formation resulted in failure of the fibers.

Post curing of the composites was done because a small exothermic peak was seen for the cured composites indicating incomplete curing, as discussed in the DSC section. No exothermic peak was seen for post cured samples. It has been reported that the impact and the hardness properties of epoxy resins reinforced with natural fibers were improved on post curing (Srinivasa and Bharath 2011). It is well-known that thorough cured thermoset composites have longer lifetime than for poorly cured composites. Though the increase in the tensile properties of the post cured composites in this work was not significant due to high standard deviation, it is important to fully cure the thermoset resin to obtain stable properties in structural composites. Partly cured resins could result in high strain at rupture due to high mobility of the polymer chains; giving a more ductile behavior than that of completely cured ones.

Impact test

Charpy impact strength (Table 1) shows the energy absorbed by the specimen during fracture. Impact strength of the specimens was between 16 and 30 kJ/m². Low impact resistance of the produced composites was expected due to alignment of the fibers in the nonwoven fabrics. This is comparable to our earlier study where nonwoven jute fiber was used as reinforcement in soybean oil based thermoset resin (Ramamoorthy et al. 2012). Similar results were obtained when using cellulose fibers in a thermoplastic polymer as reinforcement (Bledzki et al. 2009; Oksman et al. 2003), and when using a lactic acid based thermoset resin, which was impregnated in a nonwoven natural fiber mat (Åkesson et al. 2009). Our prior studies showed that the impact strength increased on changing the alignment of fibers (Ramamoorthy et al. 2012; Esmaeili et al. 2014).

Silane treatment and low concentration alkali treatment increased the impact strength whereas high concentration alkali treatment decreased the impact resistance. It is not possible to draw any conclusions, as the change is small and not statistically significant. Post-curing of the composites slightly increased the impact strength as explained in previous section (tensile properties). Impact strength followed a similar trend to that of tensile strength and modulus.

Table 2 Flexural properties of the composites with various treated conditions

Sample conditions	Flexural strength (MPa)	Flexural modulus (GPa)
Untreated ^a	115.9 ± 16.5	5.0 ± 1.3
Silane treated		
6 wt%	121.9 ± 21.1	6.2 ± 1.0
Alkali treated		
8 wt%	90.4 ± 18.3	3.2 ± 1.8
10 wt%	52.9 ± 17.4	3.0 ± 1.0

Standard deviation written after ±

Flexural test

Similarly to the tensile properties, the flexural properties of the composites, shown in Table 2, were affected by fiber surface treatments. The flexural strength and modulus of untreated fiber reinforced composites were 116 MPa and 5 GPa respectively which can be compared to the results from previous studies (Ramamoorthy et al. 2013; Esmaeili et al. 2014). On silane treatment, there was insignificant increase in flexural strength but the modulus increased by 24 %. Meanwhile, the flexural strength and the modulus fell drastically on alkali treatments. The flexural strength and modulus dwindled 54 and 40 % on highest alkali concentration. The reason for the deterioration of the mechanical properties is discussed in the previous sections. Post curing of the composites increased the flexural strength and the modulus marginally.

The data from the mechanical testing shows that the properties of the composites could be improved on appropriate chemical treatments such as silane and alkali with suitable treatment conditions. The composite could fail indeterminately due to poor interfacial adhesion between fiber and matrix as the load transfer amid the components is then ineffective. As a result of poor interfacial adhesion, crack propagation could be initiated at low stress due to brittleness of the matrix. Therefore, it is necessary to improve the interphase for good composite structures. The results from this paper and the preceding paper show that the mechanical properties are improved on surface treatment due to enhanced interfacial adhesion between fiber and matrix (Ramamoorthy et al. 2014).

Density and porosity measurements

Good resin penetration in the fabrics and the fiber structures reduce the composite porosity. Furthermore,

the composite manufacturing process also influences the porosity by trapping or releasing the air during molding. Pores, which are air filled cavities, are difficult to avoid in composites production due to the mixing of sometimes high viscosity resins, and due to dense reinforcements. Table 3 shows a summary of the density and porosity measurements of the composites. Fiber volume fraction in the composites was maintained between 42 and 45 vol% and the porosity volume was between 1 and 7 vol%. Increase in fiber volume fraction could increase the tensile strength and modulus whereas the pores develop due to improper reinforcement wetting. These porous regions could initiate the delamination of the layers resulting in composite failure. A study based on natural fiber composites showed that the porosity increased at high fiber volume fraction (Madsen and Lilholt 2003). Due to these reasons, a closely packed nonwoven structure was chosen as reinforcement for a composite with a fiber volume percent between 42 and 45 %. The pore volume was 6.4 % when the untreated fabric was used as reinforcement and falls in line with previous study on porosity prediction resulted in porosity between 4 and 8 % (Madsen and Lilholt 2003). The high pore volume could be attributed to the poor fiber–matrix interface. The treated fabrics resulted in lower porosity of the composites; porosity between 1.3 and 1.9 vol% on silane treatment while it was between 3.4 and 4.3 vol% on alkali treatment, the reason could be better interaction between fiber and matrix and improved adhesion between fiber surface and resin (introducing new moieties on silane treatment and increase surface roughness on alkali treatment). Lower porosity due to silane treatment resulted in stronger composites; as higher tensile properties were achieved, see Table 1. The decrease in the porosity could also affect the water absorption of the composites and this was explored later in this paper.

Table 3 Density and porosity of the composites with various treated conditions

Sample conditions	Density (g cm ⁻³)	Fiber volume fraction (%)	Matrix volume fraction (%)	Porosity volume fraction (%)
Untreated	1.28 ± 0.08	42.22 ± 2.7	51.38 ± 3.2	6.40 ± 0.05
Silane treated				
6 wt%	1.35 ± 0.02	44.49 ± 0.6	54.15 ± 0.8	1.36 ± 0.01
8 wt%	1.35 ± 0.04	44.55 ± 1.3	54.22 ± 1.6	1.23 ± 0.03
10 wt%	1.34 ± 0.09	44.25 ± 2.9	53.85 ± 3.6	1.90 ± 0.07
Alkali treated				
6 wt%	1.32 ± 0.04	43.43 ± 1.4	52.85 ± 1.7	3.72 ± 0.03
8 wt%	1.32 ± 0.01	43.56 ± 0.5	53.01 ± 0.6	3.43 ± 0.01
10 wt%	1.31 ± 0.04	43.18 ± 1.3	52.55 ± 1.6	4.27 ± 0.03

Standard deviation written after ±

Dynamic mechanical thermal analysis (DMTA)

DMTA results showed the viscoelastic properties of the cured resin and the composites. Storage modulus of the cured resin was 3521 MPa at 30 °C which corresponds to the polymer chain packing density in the glassy state (Bakare et al. 2014). High cross-linking density restricts the movement of the chain segments. There was drop in storage modulus between 40 and 85 °C which is due to free movement of the polymeric chain, also termed as rubbery plateau region. Loss modulus of the cured resin was 358 MPa at 30 °C and the glass transition from tan δ curve peak was nearly 90 °C for the cured resin.

Figure 3a shows storage modulus of cured resin and composites with and without surface treatments. Storage modulus increased to 4206 MPa at 30 °C on addition of fibers and this is due to the increase in stiffness of composites compared to the cured resin. The modulus increased to 4704 MPa at 30 °C on introducing silane treated fibers (6 wt% conc) as reinforcement due to good adhesion between fiber and matrix; while it fell sharply on harsh alkali treatment (10 wt% conc). These results are in a good agreement with the mechanical properties, see Tables 1 and 2.

Figure 3b presents the tan delta curves of above mentioned resin and composites; these curves indicate the damping properties. The tan delta intensity of the resin was high which demonstrates a balance between elastic and viscous behavior of the resin (good damping property) while the intensity of the tan delta peak was limited when introducing the reinforcement,

as expected. The glass transition temperature of the composites was over 100 °C; higher than that of the neat resin. T_g increase on addition of cellulosic fibers was due to restricted mobility of the polymer chains in the interphase and was observed previously by several authors (Åkesson et al. 2011; Esmaili et al. 2014).

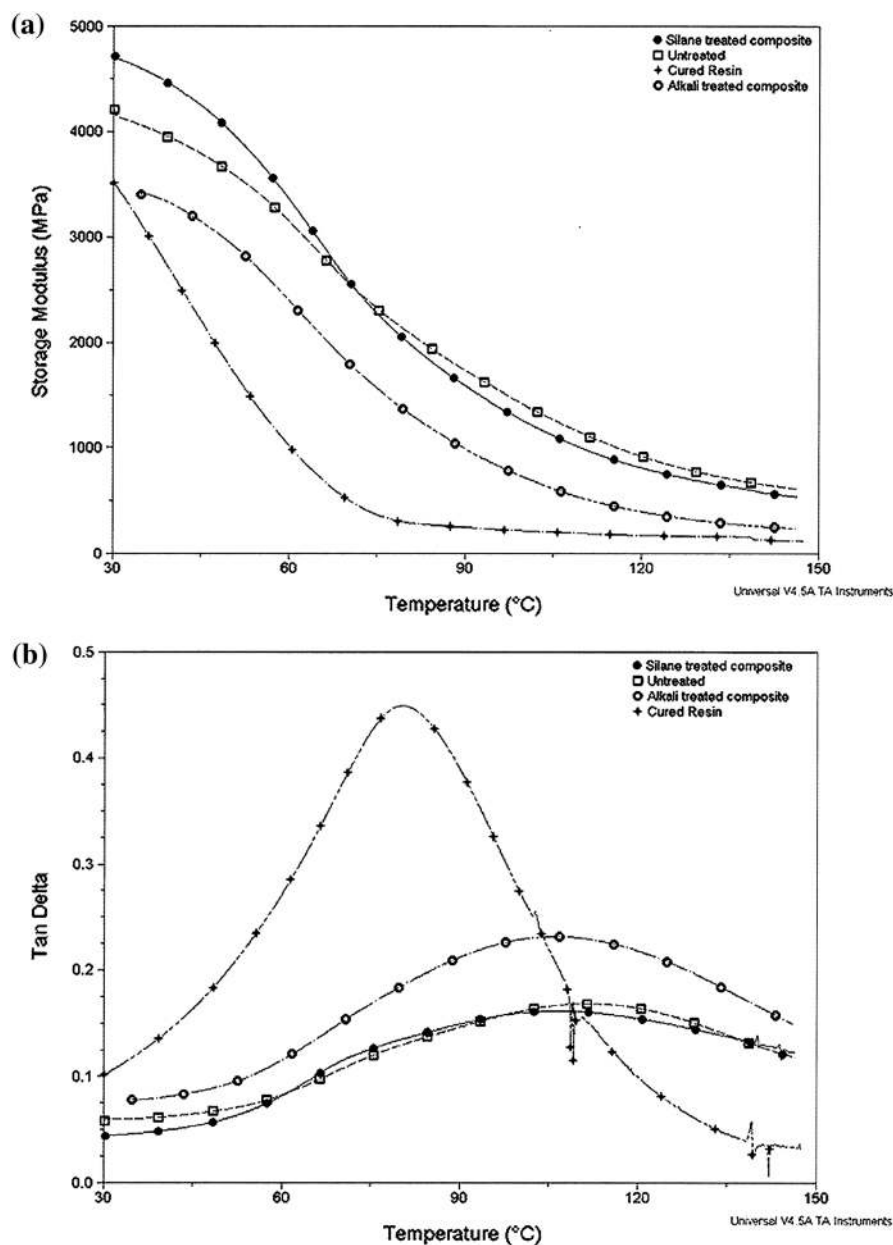
Differential scanning calorimetry and thermogravimetric analysis results were investigated to study the resin curing and thermal resistance. Thermal tests were performed to determine exothermic heat release from resin, glass transition temperature, storage modulus, loss modulus and thermal degradation.

Differential scanning calorimetry (DSC)

DSC analysis showed the crosslinking reaction efficiency of the resin at the used curing conditions and the requirement of post-curing of the composites. No exothermic peak was seen for the cured resin, which indicates complete curing of the resin whereas the uncured resin showed that 227 J/g exothermic heat evolved, see Table 4. This high exothermic heat corresponds to a high resin reactivity and short chain length. The glass transition of the cured resin was 86 °C and this was lower than T_g (90 °C) obtained from DMTA. This is mainly due to DMTA sensitivity to the glass transition.

The produced composites were characterized to monitor the resin cure, and it was found that the composites needed a post-curing as a small exothermic heat (13 J/g) peak appeared. This exothermic heat peak disappeared after the post-curing which confirms

Fig. 3 **a** Storage modulus of cured resin and composites with and without reinforcement surface treatments (silane and alkali). **b** Tan delta of cured resin and composites with and without reinforcement surface treatments (silane and alkali)



the complete curing of the composites. The tensile strength (Table 1), did not increase significantly on post-curing but it is necessary to have thorough curing of the resin in the composite to minimize the failure nodes in structural applications (Karbhari 2007). The ductility of the partially cured resins is good as the strain at break is high due to mobility of the polymer chains; consequently it reduces the tensile properties of the composites.

Thermogravimetric analysis (TGA)

Thermal decomposition resistance of the resin and the composites were analyzed by studying the gravimetric weight loss with the function of temperature. The resin was relatively stable up to 240 °C and the maximum degradation occurred after 375 °C. At 259 °C, the weight loss was about 10 % whereas 90 % weight loss and second derivative peak were at 442 and 428.5 °C

Table 4 DSC characterization results of the resin and the composites

	Exothermic heat (J/g)	T _g (°C)
Resin		
Uncured	227.4	–
Cured	0	85.8
Composite		
Before post-curing	13.0	81.8
After post-curing	0	81.7

respectively. The weight loss of the composites varied on composites due to the inclusion of cellulose fibers. Initial ten percent weight loss of the composites was mainly because of the amount of the moisture in the composites, and slight decomposition of the resin. The temperature at which 90 % of the material is lost was increased from 442 °C in the resin to 595 °C in the composites and the treatments on reinforcements did not vary the results significantly. The increase in degradation temperature for the composites compared to neat resin was mainly due to the residual ash obtained from high amount reinforcement (50 %) in the composites. Fiber surface treatment did not affect the thermal degradation, as all components of the composites degrade at high temperature. The second derivative curves showed two peaks for the composites due to degradation of reinforcement and matrix at different temperatures. The second derivative peak for the matrix was between 417 and 424 °C; and it reduced slightly in the composites whereas the peak for neat reinforcement was between 268 and 310 °C. This change in derivative peak temperature for the reinforcements is interesting as it shows the effect of surface treatments. Rapid cellulose degradation occurs at about 300 °C and this could shift on surface treatments as shown in Table 5.

Contact angle and surface energy

Polarity of the fibers and the matrix are responsible for the hydrophilicity of the composites. High contact angle value of the composites could be due to the lack of polar surface groups or that these groups have non-accessible locations. When a liquid comes in a contact with a solid surface, there is an interaction of the polar and dispersive parts of both solid and liquid phase at

Table 5 Thermal stability results from TGA characterization

	TGA		
	Temperature at 10 wt% Loss (°C)	Temperature at 90 wt% Loss (°C)	Second Derivative Peaks (°C)
Resin			
Cured	258.9	442.1	428.5
Composite			
Untreated	254.8	595.5	308.6; 417.6
Silane treated			
6 wt%	262.7	595.3	309.2; 417.3
8 wt%	258.7	595.4	302.6; 424.2
10 wt%	252.6	595.4	297.2; 423.1
Alkali treated			
6 wt%	261.1	593.2	297.4; 420.0
8 wt%	261.4	595.3	268.7; 424.8
10 wt%	262.0	595.4	285.3; 424.7

the interface. The surface tension at the interface is higher than the total surface tension of the solid and liquid phase, which is due to interactions at the interface (Ramamoorthy et al. 2014). Table 6 shows the surface energy components of the probe liquids used in the wetting experiments. The probe liquids were used to measure the contact angle (θ) and the acid–base surface energy. The contact angle is a function of the solid's surface energy and the liquid's surface tension. The contact angle below 90° represents the wetting of the solid phase whereas the angle below 90° represents the non-wettability.

The values of the contact angle with standard deviation of all composites for four probe liquids are given in Table 7. The contact angle of the composites increased when the reinforcements were treated with silane or alkali except for the 6 wt% alkali treatment. These results were coherent with previous studies when natural and regenerated cellulose fibers were surface treated with silane and alkali (Ramamoorthy et al. 2014; Park et al. 2006). The high contact angle of about 59° and 62° was achieved on treating the fibers with silane and alkali treatments respectively. There could be several reasons for the change in the contact angle such as silane molecules covering hydrophilic fiber surface, good penetration of matrix into alkali treated fiber pores, good interlocking of matrix with surface treated fibers and good interfacial adhesion between fiber and matrix. The composites are still

Table 6 Constant surface energy components of probe liquids

Solvent (heavy phase)	γ^{tot} (mN/m)	γ^{d} (mN/m)	γ^{p} (mN/m)	γ^+ (mN/m)	γ^- (mN/m)	γ^{AB} (mN/m)
Formamide	58	39	19	2.28	39.6	19
Ethylene-glycol	48	29	19	3	30.1	19
Water	72.8	21.8	51	25.5	25.5	51
Hexadecane	27.47	27.47	0	0	0	–

Light phase—air

Table 7 Contact angles with standard deviation of the composites using optical tensiometer

Conditions	Contact angle (θ)			
	Water	Formamide	Ethylene-glycol	Hexadecane
Untreated	42.4 \pm 4.7	18.3 \pm 3.6	33.3 \pm 2.1	10.0 \pm 1.9
Silane treated				
6 wt%	45.3 \pm 4.5	21.8 \pm 2.9	25.1 \pm 3.1	18.8 \pm 1.1
8 wt%	52.1 \pm 3.6	24.0 \pm 2.0	33.0 \pm 2.8	20.8 \pm 5.8
10 wt%	58.6 \pm 5.3	36.2 \pm 6.8	37.0 \pm 4.2	26.7 \pm 3.0
Alkali treated				
6 wt%	36.8 \pm 3.4	20.7 \pm 3.6	27.7 \pm 2.0	18.6 \pm 2.3
8 wt%	61.8 \pm 3.5	36.8 \pm 4.3	37.0 \pm 4.2	21.4 \pm 1.7
10 wt%	62.2 \pm 1.1	41.3 \pm 4.0	42.7 \pm 4.0	26.9 \pm 3.6

hydrophilic as the contact angle of the composites is lower than 90°; this outcome supports the results from water absorption. Nevertheless, the change in contact angle clearly indicates the change in hydrophilicity of the composites on surface treatments with silane and alkali.

The total surface free energy, γ^{tot} , is the sum of dispersive (γ^{d}) and the polar components (γ^{p}). The dispersive and polar surface energies are measured by Owens–Wendt equation,

$$\gamma_{\text{L}}(1 + \cos \theta) = 2(\gamma^{\text{dS}}\gamma^{\text{dL}})^{1/2} + 2(\gamma^{\text{pS}}\gamma^{\text{pL}})^{1/2} \quad (8)$$

where γ_{L} , γ^{dL} (dispersive) and γ^{pL} (polar) are known surface energies of test liquids and γ^{dS} and γ^{pS} are surface energies of the solid which are calculated from the measured contact angles.

The acid–base component (hydrogen bonding), γ^{AB} , includes electron acceptor (γ^+) and electron donor (γ^-) components. It is calculated by

$$\gamma^{\text{AB}} = 2(\gamma^+\gamma^-)^{1/2} \quad (9)$$

Table 8 shows the surface energy components of the composites. The surface energy decreased on

Table 8 Acid–base surface energy components of the composites

Conditions	γ^{tot}	γ^{d}	γ^{p}	$\text{sqrt}(\gamma^+)$	$\text{sqrt}(\gamma^-)$
Untreated	54.3	9.4	44.9	4.0	5.5
Silane treated					
6 wt%	53.2	9.0	44.2	4.3	5.1
8 wt%	47.3	9.9	37.4	4.2	4.5
10 wt%	41.8	10.1	31.7	3.9	4.1
Alkali treated					
6 wt%	59.2	8.0	51.2	4.2	6.0
8 wt%	39.1	11.6	27.5	3.8	3.6
10 wt%	38.7	10.8	27.9	3.5	3.9

The values are calculated from the mean values in Table 7

silane and alkali treatments; except when the fiber was treated with 6 wt% concentration alkali. The decrease in the surface energy indicates the increase in hydrophobicity. The results follow the outcome from the contact angles. The decrease of the basic component, γ^- , of the surface energy indicates the reduction of hydroxyl groups. The silane treatment reduces the γ^- as the hydroxyl groups were covered by silane

coupling agents. The surface energy and the contact angle of the neat fibers were investigated our previous study (Ramamoorthy et al. 2014). The results of the fiber and the composite fall in line with each other; with these results further investigations on work of adhesion could be done (Park et al. 2006).

Water absorption

Water absorption of the composites was followed for 10 days and it was found that the absorption was more pronounced for the first 5 days. The absorption was minor after first 5 days as observed previously with cellulose fiber composites (Ramamoorthy et al. 2012). The absorption of the composites was primarily influenced by the cellulose reinforcement (Esmaili et al. 2014). It could also be influenced by diffusion of water molecules between the polymer chain, into the pores and into the fiber–matrix interface. So, it is necessary to use less hydrophilic

fibers and a resin with higher cross-linking density. The silane and alkali treatments on reinforcements, and their concentrations affected the water absorption of the composites, see Fig. 4. The silane treatment, 10 wt% concentration, reduced the water absorption of the composites from 33 to 23 wt% while the reduction was not conspicuous on alkali treatment for same concentration. The reduction could be due to two reasons, namely the chemical modification in the fiber and the interfacial changes in the composites. These results were in line with porosity measurements and mechanical properties. The mechanical properties, strength and modulus, of the composites deteriorated after absorption and this was in an agreement with former study (Ramamoorthy et al. 2012). The percentage decrease in tensile properties is tabulated in Table 9. The tensile strength and modulus fell 79 and 66 % respectively on alkali treatment while this was lower on silane treatment, 51 and 58 % correspondingly.

Fig. 4 Water absorption (wt%) of the composites after 10 days immersion in water

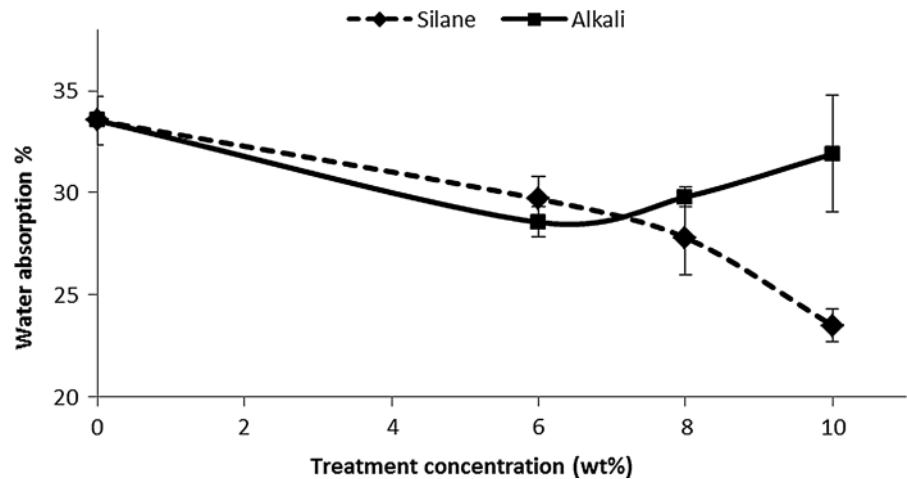


Table 9 Water absorption of the composites with various treated conditions

Sample conditions	% Reduction in tensile properties after water absorption	
	Tensile strength (%)	Young's modulus (%)
Silane treated		
6 wt%	34.4	49.4
8 wt%	45.8	59.9
10 wt%	51.0	58.2
Alkali treated		
6 wt%	64.2	56.3
8 wt%	65.9	59.7
10 wt%	79.4	65.8

The percentage reduction is calculated from the mean strength and modulus before and after water absorption

Microscopy

Figure 5 shows the SEM micrographs of tensile fractured surface before and after water absorption. Untreated fiber reinforced composite before water absorption (a) had pores at the interface and fiber pull out was noticed whereas silane treated composite (b) was well embedded in the matrix and had smaller

fiber pull out. This ratifies the increase in tensile strength and modulus, and decrease in elongation on silane treatment (Table 1). Alkali treated composite (c) had pores and fiber damage which confirms the decrease in tensile properties on alkali treatment. The fiber damage resulted in low elongation due to failure of fiber and composites at low strain. These deductions go together with the results from porosity and water absorption.

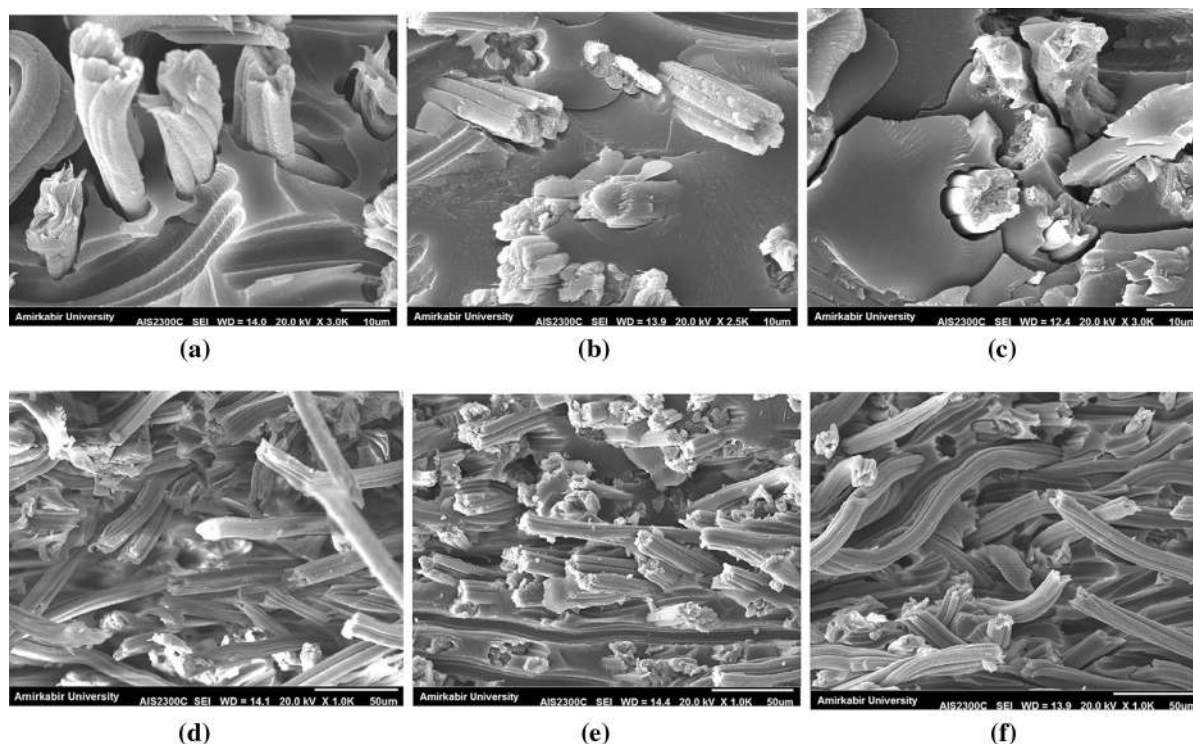


Fig. 5 SEM images of tensile fractured composites; before water absorption **a** untreated, **b** silane 10 wt%, **c** alkali 10 wt%; after water absorption **d** untreated, **e** silane 10 wt% **f** alkali 10 wt%

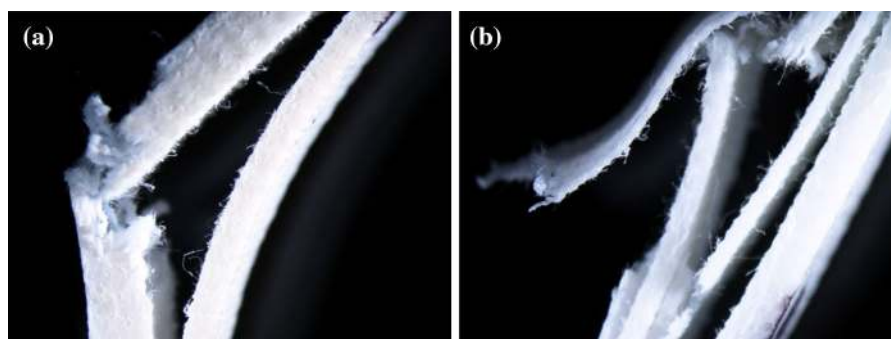


Fig. 6 Optical microscopy images of tensile fractured composites after water absorption **a** silane 10 wt% **b** alkali 10 wt% treated fiber reinforced composites

Fig. 7 Resonance analysis using Audacity and Scilab **a** sound data, amplitude vs time, obtained using Audacity **b** frequency data converted from sound data, amplitude intensity versus frequency **c** graph plotted, frequency against different length

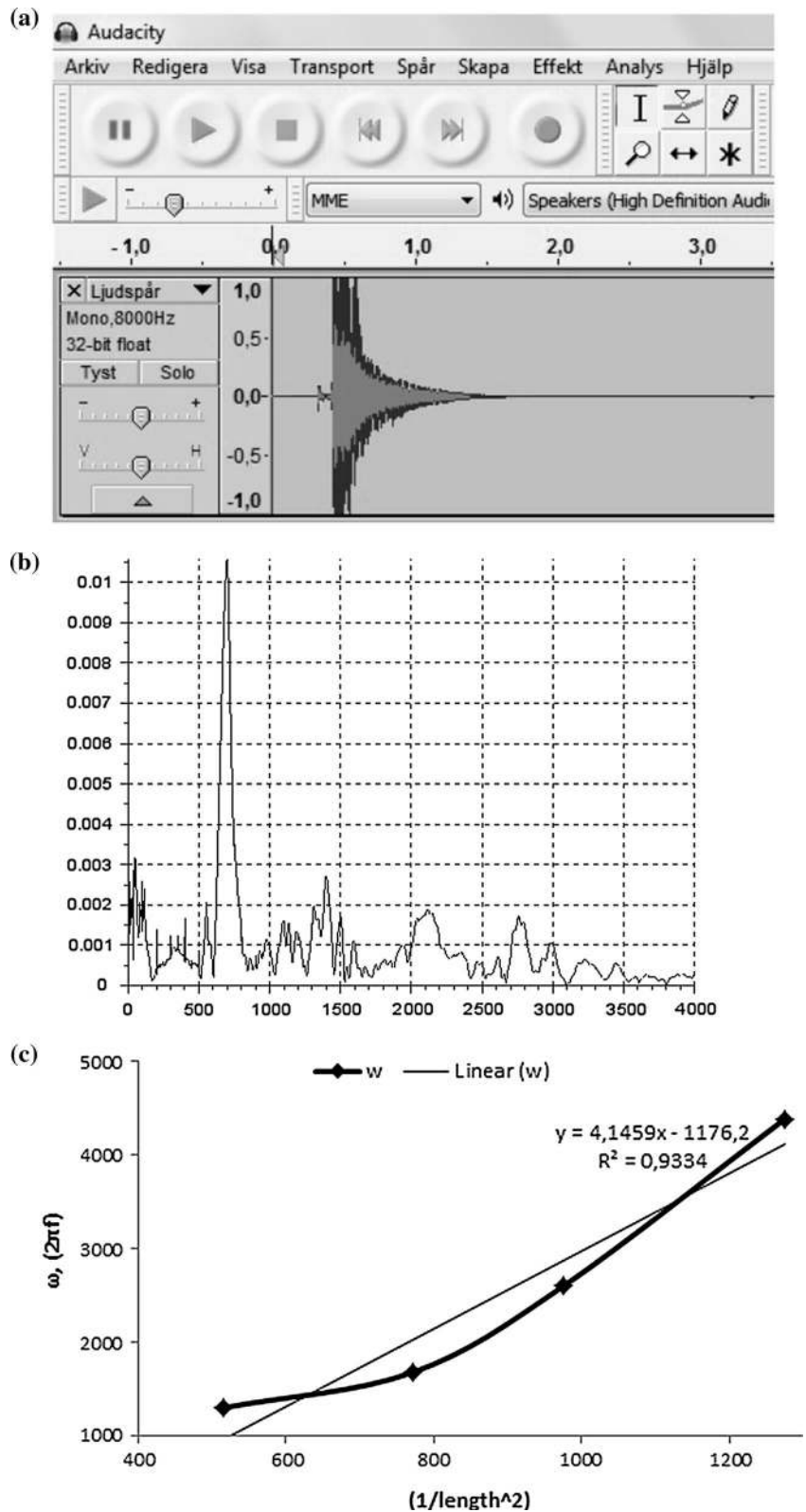


Table 10 Thermal conductivity, diffusivity and specific heat measured using TPS 2500 hot disk

Composite	Conductivity (W/m K)	Diffusivity (mm ² /s)	Specific heat (MJ/m ² K)
Untreated	0.363	0.284	1.29
Silane 8 wt%	0.400	0.333	1.20
Alkali 8 wt%	0.379	0.296	1.28

Water absorbed specimens behaved differently during tensile test, Fig. 5d–f. There was long fiber pull out for all specimens after water absorption; which reduced the tensile strength and modulus (Table 9), and increased the elongation.

Optical microscopy images were taken to see the behavior of layers on water absorbed tensile fractured specimens. The delamination of layers was noticed on treated water absorbed specimens. The reduction of tensile properties (Table 9) was partly due to delamination caused by water absorption at interface. This also confirms the water absorption at interface (Fig. 6).

Resonance analysis

The modulus calculated using this non-destructive method was of insignificant difference to the modulus obtained from destructive tensile test, which conclude that both approaches lead to a correct estimate of Young's modulus. The acoustic signals of the vibrating composite beam were detected as a function of amplitude to time, as shown in Fig. 7a. Harmonic oscillations on displacing the beam (mechanical vibrations) were converted into an electrical signal using piezoelectric transducer before the signals were recorded by the sound card in Audacity. The time data was converted into frequency by a fast Fourier transform (FFT) using Scilab, as shown in Fig. 7b. The script used to execute the FFT is shown in characterization section. Tests were repeated with the different beam fastening lengths and the obtained graph was plotted as show in Fig. 7c. The slope obtained from the Fig. 7d and the modulus was calculated from Eq. 4.

The modulus of the 8 and 10 wt% concentration alkali treated fiber composites was 7.2 and 6.7 GPa respectively on non-destructive analysis, whereas the same composites yielded 7.8 and 6.9 GPa on destructive tensile testing. Likewise, the modulus of the silane

treated fiber composites was in agreement with tensile testing. Similar analysis was performed on concrete slabs as a part of French national research project (Villain et al. 2011). Resonance analysis can also be used to determine the fiber debonding, delamination, cracking and micro-failure mechanism inside the composite structure (Park et al. 2006). It is also known that torsional vibrations yield shear modulus of the composites.

Thermo-physical test

Table 10 shows the bulk thermo-physical properties of the composites. Thermal conductivity, thermal diffusivity and specific heat were measured simultaneously at constant temperature as these properties were largely affected by temperature. There was an increase in the conductivity and diffusivity of the composites on fiber surface treatment, whereas the specific heat of the composites decreased on treatments. This was in agreement with our previous study on fibers where the C_p was reduced from 1.66 and 1.25 to 1.19 and 0.99 J/g C on alkali and silane treatments respectively (Ramamoorthy et al. 2014). Thermal conductivity of natural fibers and thermoset acrylic resins has been studied previously by Behzad and Sain (2007). Thermal conductivity of the resin (0.43 W/m K) was lower than that of the fiber (1.48 W/m K). The composite produced in our study possess low thermal conductivity, 0.363 W/m K, when the fabric was reinforced without any treatment. The low conductivity was mainly due to the fact that 50 % of the composites were thermoset matrix. On silane and alkali treatment, the conductivity was 0.4 and 0.38 W/m K respectively. These results were in line with oil palm fiber reinforced phenolformaldehyde composites where the conductivity of the composites (0.29 W/m K) was increased when the reinforcing fiber was treated with silane (0.46 W/m K) and alkali (0.42 W/m K) (Agrawal et al. 2000). The increase on silane treatment could be due to silane molecules available on fiber surface, which make the fiber less hydrophilic and increases the adhesion between the treated fiber and thermoset matrix. It can also be due to the increase in the polarity due to the presence of Si–OH group. Alkali treatment also increased the thermal conductivity, which could be a result of improved adhesion between fiber and matrix as the OH groups react with NaOH and gives rough surface topography. The

change in the fiber's surface roughness and increase in diameter was noticed using microscopy images in our preceding study (Ramamoorthy et al. 2014). Similar fiber behavior on surface treatment was noticed in this study. The pores created on alkali treatment allow good interlocking with the matrix to increase the thermal conductivity.

Thermal diffusivity of the composites also increased on fiber treatments and this was in good agreement with oil palm fiber reinforced phenol-formaldehyde composites (Agrawal et al. 2000). The specific heat capacity of the composites decreased on fiber treatment, which shows that lower energy was required to heat the composites after treatment. Heat capacity of the treated fibers was discussed in our preceding study (Ramamoorthy et al. 2014).

Finite element analysis

From our preceding study, it was found that the C_p of the regenerated cellulose fiber was reduced from 1.66 and 1.25 to 1.19 and 0.99 J/g °C on alkali and silane treatments respectively (Ramamoorthy et al. 2014). The specific heat increased as the temperature rose from 30 to 50 °C. Hemp fiber showed similar increase in C_p from 2.2 J/g K to almost 3.4 J/g K when the temperature rose from 20 to 100 °C (Behzad and Sain 2007). Similarly, the specific heat of the cured resin increased with temperature and could be fitted in second order polynomial as explained by Behzad and Sain (2007).

Composite was modeled in COMSOL 4.3b with same amount of fiber and resin as in the experiment. This simulation was carried out on some assumptions; composite laminate is free of voids, heat loss due to radiation and convection is neglected, fibers are uniform (shape and size), aligned uni-directionally and thermal contact resistance between fiber and matrix interface is negligible. The study was done with heat transfer module in time dependent model by employing the experimental values of thermal conductivity and specific heat (transverse direction—across the fiber). The temperature variation with time at different locations was obtained. It was noted that the predicted temperature data was in agreement with the measured data with slight disparity, and similar results were obtained with hemp fiber reinforced composites (Behzad and Sain 2007). Thermal conductivity of the composites could be also predicted by

E–S model as explained by Behzad and Sain (2007). As expected, the results changed when the model was studied along the fiber (in-plane direction) and when the amount of fiber increased/decreased in the composites.

However, the numerical results in this paper are limited as the moisture uptake resulting in property degradation and the large variation of the fiber properties after treatment was not considered. Detailed numerical study of the hemp fiber composite's moisture uptake and mechanical properties was done by Toubal et al. (2015) which will be considered in our future research.

Conclusions

Detailed study of biocomposites produced from regenerated cellulose fibers and lab synthesized resin was discussed in order to improve the interface and composite properties. Regenerated cellulose fibers were treated with silane and alkali and their properties were thoroughly discussed in our preceding work (Ramamoorthy et al. 2014) and the resin was characterized in our former study (Bakare et al. 2014). Biocomposites were manufactured by reinforcing untreated and treated regenerated cellulose fibers in novel lab synthesized bioresin (78 % bio content) from glycerol and lactic acid by direct condensation and functionalization. Tensile, flexural and impact tests were used to evaluate the mechanical properties of the composites whereas DMTA was used to evaluate viscoelastic properties. The composites had good mechanical properties and the properties were improved by some treatments. Highest tensile strength (91 MPa) and modulus (9.5 GPa) were obtained when the fiber was treated with silane. The improvement on silane treatment was due to molecular continuity formed in the interphase of the composite as silane molecules can form siloxane bridges between the cellulose fiber and the resin. Alkali treatments also altered the properties which is mainly due to increase in surface roughness and hydrogen bonding disruption. Higher strength could be obtained by changing the fabric architecture as discussed in our previous study (Esmaeili et al. 2014). Hybridization could also improve the properties as discussed in former study (Ramamoorthy et al. 2012). The results from the impact and the flexural tests fall in line with the tensile

test results; highest impact strength (28 kJ/m²), flexural modulus (122 MPa) and flexural strength (6.2 GPa) were obtained when the fibers were treated with silane. Highest viscoelastic properties were achieved for the composites reinforced with silane treated fibers and follow the results from the mechanical tests. Glass transition temperature of the composites was measured from DMTA tan delta curves and was over 100 °C. Archimedes principle was used to determine density and porosity measurements. Porosity volume of the composites reduced from 6.4 to 1.2 and 3.4 % on silane and alkali treatment respectively. This was due to interface improvement as the fibers were well embedded in the matrix. Thermal properties were assessed by DSC and TGA. The curing of the resin was followed using DSC and the composites were subjected to post-curing based on DSC results. The glass transition temperature of synthesized resin was higher than thermoplastic PLA. Glass transition from DSC was lower than that of DMTA due to the sensitivity of DMTA. Thermal degradation was followed using TGA and the change in the second derivative peak showed that the treatments altered the stability of the reinforcement. The hydrophilicity of the composites was evaluated using contact angle, surface energy and water absorption. Fiber treatment changed the hydrophilicity of the composites and this was due to changes in the fibers and interface. Water absorption decreased the tensile properties of the composites as expected. Morphological analysis performed using microscopy images. These images show the good interface between silane treated fiber and matrix whereas the untreated fiber composites had pores at interface. This indicated better adhesion between fiber and resin on silane treatment. The fiber damage was noticed on high alkali concentration and long fiber pull out was noticed on water absorbed specimens. These results get along with the tensile properties. Thermal conductivity, diffusivity and specific heat were measured for the composites, and it was found that the treatment improved the conductivity and diffusivity as anticipated. Non-destructive method, resonance analysis, was used to measure modulus of the composites by converting the acoustic signals of the vibrating composite beam to electrical signals with piezoelectric transducer. The modulus was similar to the results from the destructive tensile testing. Finite element analysis was used to predict the thermal behavior of

the composites. The temperature variation obtained from simulation was comparable to the experimental results regardless of some assumptions. However, the modeling in this paper was limited as the moisture uptake resulting in property degradation and the large variation of the fiber properties after treatment was not considered.

The results from this paper show the potential to use the previously reported novel bioresin and helps in choosing a surface treatment for cellulose fibers intended for composites. This paper also shows the potential of regenerated cellulose fibers in structural composites. The properties of these composites could be further enhanced by changing the textile architecture and physical characteristics of the reinforcements as discussed in our previous study, and can be used in various non-structural applications (Esmaeili et al. 2014). The changes in the composite properties were due to the changes in fiber surface and interface. Previous research on surface modified natural fibers showed better performance in composite production and their properties due to the change in hydrophilicity of the fiber and fiber–matrix adhesion. These composites were subsequently used in composite applications. In our upcoming project, the stability of the cellulose composites on water absorption will be focused. On further improvement, regenerated cellulose fiber reinforced composites could also be used in several composite applications.

Acknowledgments This research was funded by research foundation ÅForsk, Sweden. Authors would like to thank Adib Kalantar for assisting in thermal conductivity measurements.

References

- Adekunle K, Patzelt C, Kalantar A, Skrifvars M (2011) Mechanical and viscoelastic properties of soybean oil thermoset reinforced with jute fabrics and carded lyocell fiber. *J Appl Sci* 122:2855–2863
- Adusumali RB, Reifferscheid M, Weber H, Roeder T, Sixta H, Gindl W (2006) Mechanical properties of regenerated cellulose fibres for composites. *Macromol Symp* 244:119–125
- Agrawal R, Saxena NS, Sreekala MS, Thomas S (2000) Effect of treatment on the thermal conductivity and thermal diffusivity of oil-palm-fiber-reinforced phenolformaldehyde composites. *J Polym Sci Part B Polym Phys* 38:916–921
- Åkesson D, Skrifvars M, Seppälä J, Turunen M, Martinelli A, Matic A (2009) Processing of structural composites from biobased thermoset resins and natural fibres by compression moulding. *J Biobased Mater Bioeneg* 3:215–225

- Åkesson D, Skrifvars M, Seppälä J, Turunen M, Martinelli A, Matic A (2010) Synthesis and characterization of a lactic acid-based thermoset resin suitable for structural composites and coatings. *J Appl Sci* 115:480–486
- Åkesson D, Skrifvars M, Seppälä J, Turunen M (2011) Thermoset lactic acid-based resin as a matrix for flax fibers. *J Appl Sci* 119:3004–3009
- Bakare FO, Skrifvars M, Åkesson D, Wang Y, Afshar SJ, Esmaeili N (2014) Synthesis and characterization of bio-based thermosetting resins from lactic acid and glycerol. *J Appl Polym Sci*. doi:10.1002/app.40488
- Behzad T, Sain M (2007) Measurement and prediction of thermal conductivity of hemp fibre reinforced composites. *Polym Eng Sci* 47:977–983
- Bledzki AK, Gassan J (1999) Composites reinforced with cellulose based fibres. *Progr Polym Sci* 24:221–274
- Bledzki AK, Reihmane S, Gassan J (1996) Properties and modification methods for vegetable fibers for natural fiber composites. *J Appl Polym Sci* 59:1329–1336
- Bledzki AK, Jaszkiwicz A, Scherzer D (2009) Mechanical properties of PLA composites with man-made cellulose and abaca fibres. *Compos Part A* 40:404–412
- Bravo A, Toubal L, Koffi D, Erchiqui F (2015) Development of novel green and biocomposite materials: tensile and flexural properties and damage analysis using acoustic emission. *Mater Design* 66:16–28
- Carrillo F, Colom X, Canavate X (2010) Properties of regenerated cellulose lyocell fiber-reinforced composites. *J Reinf Plast Compos* 29:359–371
- Caulfield DF, Feng D, Prabawa S, Young RA, Sanadi AR (1999) Interphase effects on the mechanical and physical aspects of natural fiber composites. *Angew Makromol Chem* 272:57–64
- Esmaeili N, Bakare FO, Skrifvars M, Afshar SJ, Åkesson D (2014) Mechanical properties for bio-based thermoset composites made from lactic acid, glycerol and viscose fibers. *Cellulose*. doi:10.1007/s10570-014-0500-3
- Faruk O, Bledzki AK, Fink HP, Sain M (2012) Biocomposites reinforced with natural fibers: 2000–2010. *Progr Polym Sci* 37:1552–1596
- Fink HP, Ganster J, Lehmann A (2014) Progress in cellulose shaping: 20 years industrial case studies at Fraunhofer IAP. *Cellulose* 21:31–51
- Ganster J, Fink HP (2006) Novel cellulose fibre reinforced thermoplastic materials. *Cellulose* 13:271–280
- Jaturapiree A, Manian AP, Bechtold T (2006) Sorption studies on regenerated cellulose fibers in salt–alkali mixtures. *Cellulose* 13:647–654
- Jawaid M, Abdul Khalil HPS (2011) Cellulosic/synthetic fibre reinforced polymer hybrid composites: a review. *Carbohydr Polym* 86:1–18
- John MJ, Anandjiwala RD (2008) Recent developments in chemical modification and characterization and characterization of natural fiber-reinforced composites. *Polym Compos* 29:187–207
- Johnson RK, Zink-Sharp A, Rennecker SH, Glasser WG (2008) Mechanical properties of wetlaid lyocell and hybrid fiber-reinforced composites with polypropylene. *Compos Part A Appl Sci Manuf* 39:470–477
- Karbhari VM (ed) (2007) Durability of composites for civil structural applications. Woodhead Publishing, CRC Press, Florida, p 61
- Koronis G, Silva A, Fontul M (2013) Green composites: a review of adequate materials for automotive applications. *Compos Part B* 44:120–127
- La Mantia FP, Morreale M (2011) Green composites: a brief review. *Compos Part A* 42:579–588
- Madsen B, Lilholt H (2003) Physical and mechanical properties of unidirectional plant fibre composites—an evaluation of the influence of porosity. *Compos Sci Technol* 62:1265–1272
- Madsen B, Thygesen A, Lilholt H (2007) Plant fibre–porosity and volumetric interaction. *Compos Sci Technol* 67:1584–1600
- Mohanty AK, Misra M, Drzal LT (2001) Surface modifications of natural fibers and performance of the resulting biocomposites: an overview. *Compos Interf* 8:313–343
- Oksman K, Skrifvars M, Selin JF (2003) Natural fibres as reinforcement in polylactic acid (PLA) composites. *Compos Sci Technol* 63:1317–1324
- Okubayashi S, Bechtold T (2005) Alkali uptake and swelling behaviour of lyocell fiber and their effects on crosslinking reaction. *Cellulose* 12:459–467
- Park JM, Quang ST, Hwang BS, DeVries KL (2006) Interfacial evaluation of modified jute and hemp fibers/polypropylene (PP)-maleic anhydride polypropylene copolymers (PP-MAPP) composites using micromechanical technique and non-destructive acoustic emission. *Compos Sci Technol* 66:2686–2699
- Puglia D, Biagiotti J, Kenny JM (2005) A review on natural fibre-based composites—part II: application of natural reinforcements in composite materials for automotive industry. *J Nat Fib* 1:23–65
- Ramamoorthy SK, Di Q, Adekunle K, Skrifvars M (2012) Effect of water absorption on mechanical properties of soybean oil thermosets reinforced with natural fibers. *J Reinf Plast Compos* 31:1191–1200
- Ramamoorthy SK, Kundu CK, Adekunle K, Bashir T, Skrifvars M (2013) Properties of green composites with regenerated cellulose fiber and soybean-based thermoset for technical applications. *J Reinf Plast Compos*. doi:10.1177/0731684413504325
- Ramamoorthy SK, Skrifvars M, Rissanen M (2014) Effect of alkali and silane surface treatments on regenerated cellulose fibre type (Lyocell) intended for composites. *Cellulose*. doi:10.1007/s10570-014-0526-6
- Ramamoorthy SK, Skrifvars M, Persson A (2015) A review of natural fibers used in biocomposites: plant, animal and regenerated cellulose fibers. *Polym Rev* 55:107–162. doi:10.1080/15583724.2014.971124
- Saevey KC, Ghosh I, Davis RM, Glasser WG (2001) Continuous cellulose fiber-reinforced cellulose ester composites I. Manufacturing options. *Cellulose* 8:149–159
- Seniha Güner F, Yağci Y, Tuncer Erciyes A (2006) Polymers from triglyceride oils. *Progr Polym Sci* 31:633–670
- Srinivasa CV, Bharath KN (2011) Impact and hardness properties of areca fiber–epoxy reinforced composites. *J Mater Environ Sci* 2:351–356
- Toubal L, Cuillière JC, Bensalem K, Francois V, Gning PB (2015) Hygrothermal effect on moisture kinetics and mechanical properties of hemp/polypropylene composite: experimental and numerical studies. *Polym Compos*. doi:10.1002/pc.23414

Villain G, Marrec LL, Rakotomanana L (2011) Determination of bulk elastic moduli of various concretes by resonance frequency analysis of slabs submitted to impact echo. *Eur J Environ Civ Eng* 15:601–617

Woodings C (ed) (2001) *Regenerated cellulose fibres*. Woodhead Publishing, CRC Press, Boston. ISBN 978-1-85573-459-3